# Phonon-assisted dynamical Coulomb blockade in a thin suspended graphite sheet

A. Chepelianskii, P. Delplace, A. Shailos, A. Kasumov, R. Deblock, M. Monteverde, C. Ojeda-Aristizabal, M. Ferrier, S. Guéron, and H. Bouchiat

*Laboratoire de Physique des Solides, CNRS, Université Paris-Sud, UMR 8502, F-91405 Orsay Cedex, France*

(Received 11 May 2009; published 16 June 2009)

The differential conductance in a suspended few layered graphene sample is found to exhibit a series of quasiperiodic sharp dips as a function of bias at low temperature. We show that they can be understood within a simple model of dynamical Coulomb blockade where energy exchanges take place between the charge carriers transmitted through the sample and a dissipative electromagnetic environment with a resonant phonon mode strongly coupled to the electrons.

DOI: 10.1103/PhysRevB.79.235418 PACS number(s): 63.22.Np, 73.23.Hk

## I. INTRODUCTION

One of the great challenges of molecular electronics is to access electron-phonon coupling within a single molecule. Mechanically tunable atomic break junctions with trapped small molecules such as $H_2$, $D_2$, and $H_2O$ exhibit a spectroscopic signature of their characteristic phonon modes.[1] The signature of phonons is also spectacular in the Coulomb blockade regime in molecular single electron transistors. The usual resonant tunneling conductance peaks as a function of gate or source-drain voltage are surrounded by satellites, which correspond to the emission or absorption of one or several phonons. Specific vibrational modes were thus identified in fullerenes and suspended carbon nanotubes.[2–4] Theoretical models[5–7] were developed to describe these vibrational side bands in molecular transistors. In all these investigations the single level spacing within the molecule is larger than the energy of the vibration modes, so that only a single molecular level needs to be considered. In this work we investigate the opposite limit of a mesoscopic dot where both single level spacing and Coulomb charging energy are smaller than the energy of the phonon mode considered. Moreover the transmission of the electrodes corresponds to an intermediate tunneling regime described by the physics of dynamical Coulomb blockade (DCB) through a tunnel junction in series with a dissipative environment. The samples are micron size few atomic layer graphite foils suspended between two platinum electrodes. The differential conductance exhibits at low temperature a power-law increase around zero-bias characteristic of DCB through the contacts. The graphite foil sample itself constitutes the electromagnetic environment. More original, on the thin samples a series of periodic replica of this Coulomb blockade anomaly was detected at multiples of 20 meV, corresponding approximately to the lowest energy out-of-plane optical mode in graphite (ZO').[8] These conductance dips were not observed on two control graphite samples which were likewise suspended, had similar resistance and lateral dimensions but were over 30 times thicker. We analyze these results with a simple model, inspired by Ref. 7, of a mesoscopic island connected to electrodes via tunnel barriers. We model the island by a continuous electronic spectrum coupled to a single phonon mode, which leads to an oscillating transmission of the barriers at the contacts.[7] This model can also be solved using the so-called $P(E)$ theory[9] to describe energy exchanges of a Coulomb blocked tunnel junction with a dissipative electromagnetic environment and presents a striking analogy with the behavior of a tunnel junction coupled to an electromagnetic resonator in series with an Ohmic environment investigated in Ref. 10.

## II. EXPERIMENTAL RESULTS ON SUSPENDED UNGATED SAMPLES

The samples of typical size between 2 and 3 $\mu$m were prepared by exfoliation of a highly oriented pyrolytic graphite single crystal and deposition across a 1 $\mu$m wide slit etched in a silicon nitride membrane separating two Pt contacts. The number of graphene layers was estimated from transmission electron microscopy pictures; see Fig. 1 for the thinnest samples, which contain less than 30 layers. Electrical connection was achieved simply by pressing the sample onto the electrodes. Thus the sample resistance, $R_t = 100$ k$\Omega$ at 4.2 K, mainly consists of the resistance at the

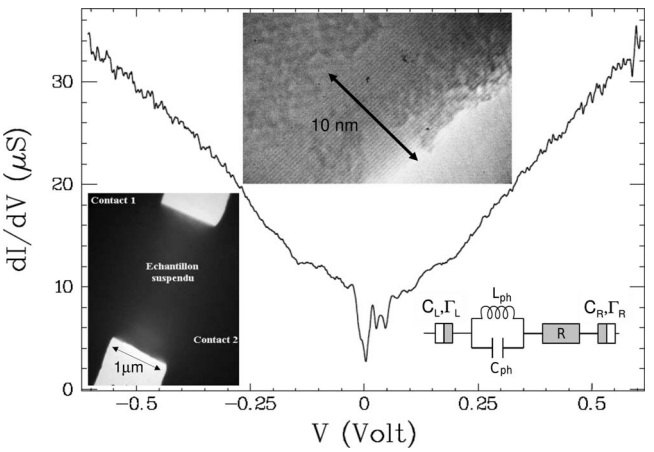


FIG. 1. Bias dependence of the differential conductance measured on a suspended thin foil of graphite. Insets: left transmission electron microscopy picture of the sample. Up: side view taken at high resolution from which it is possible to estimate the number of graphene layers of the order of 30. Right: schematic representation of the graphite sample resistance $R$ in series with a $LC$ circuit representing the Z0' phonon mode and the two asymmetrical poorly conducting electrodes.

 

contact, and increases as the temperature is reduced. The sheet resistance of the graphite layer itself is smaller than 5 kΩ, the maximal resistance of a single graphene sheet. The differential conductance $dI/dV$ was either measured by modulating the voltage bias and measuring the current modulation by standard lock-in detection or deduced from the differential resistance obtained by applying a small ac current $I_{ac}$ of typical amplitude 1–10 nA superimposed to a dc current bias $I$ up to 1 $\mu$A. The dc voltage drop $V$ through the sample was then deduced by integration of $dV/dI=f(I)$. The triangular shape of $dI/dV=f^{-1}(V)$ observed at high bias (above 0.15 V, see Fig. 1) can be related to the linear dependence of the density of states $\nu(E)$, characteristic of the band structure of graphene as well as of graphite at high enough energy.[11] Indeed, the electronic transmission between the graphite sample and the electrodes is low, so that the chemical potential can be considered as uniform along the graphite sheet equal to $E_F$. This remains true in the presence of moderate disorder in the graphite sheet. The voltage drops $V$ mainly at the contacts whose chemical potential relative to $E_F$ are respectively given by $\alpha eV$ and $(1-\alpha)eV$. The parameter $1/2 \leq \alpha \leq 1$ characterizes the asymmetry of the contact resistances and voltage drop with $\alpha=1/2$ corresponding to symmetrical contacts. Neglecting Coulomb blockade effects, the zero-temperature differential conductance can then be written as the sum of the contributions of the carriers injected from both electrodes:

$$dI/dV \propto \Gamma_L \Gamma_R [\alpha \nu(E_F + \alpha eV) + (1-\alpha)\nu(E_F - (1-\alpha)eV)], \tag{1}$$

where $\Gamma_L$ and $\Gamma_R$ are the transmissions of the left and right contacts, respectively. The asymmetry between positive and negative bias is attributed to a combination of a slight doping of the sample and some asymmetry in the transmission of the electrodes.

We now focus on the conductance at low voltage (below 10 meV), which exhibits a pronounced dip at zero bias not described by expression (1). This behavior observed in all investigated samples is characteristic of Coulomb blockade through a small capacitance tunnel junction in series with a dissipative electromagnetic environment which can exchange energy with the tunneling quasiparticles on a scale much smaller than the charging energy. This yields the so-called DCB.[9] The low-energy differential conductance is expected to follow a scaling behavior as a function of $V$ and $T$:

$$G(V) = dI/dV = T^z f(eV/k_B T), \tag{2}$$

with $\lim_{x\to 0} f(x)=C$, where $C$ is a constant and $\lim_{x\to\infty} f(x) = x^z$. The exponent $z$ is expected to be $\alpha^2 R/R_Q$ in the case of two asymmetric junctions, where $R$ is the resistance of the environment and $R_Q=h/2e^2$ is the resistance quantum. The data shown in Fig. 2 yield $z$ of the order of $0.25 \pm 0.05$. Such a power-law dependence also was found in other samples with similar exponents. It is thus reasonable to assume that the dissipative Ohmic environment in the present case is constituted by the graphene layers connected to the electrodes. A similar behavior was already observed on multiwall carbon nanotubes with low conductance contacts.[12]

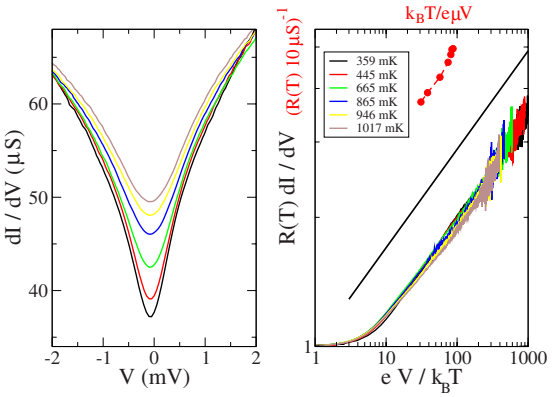


FIG. 2. (Color online) Left: differential conductance in the vicinity of zero bias measured on a thick suspended graphite sample measured at several temperatures between 300 mK (lower curve) and 1 K (upper curve). Right: the data can be rescaled according to Eq. (2) with $z=0.25$. Full circles: temperature dependence of the zero bias resistance. The continuous line is a power law of exponent 0.25.

In the following we discuss the bias dependence (below 0.1 V) of the differential conductance measured on the sample investigated which is 10 nm thick and contains $n_g=30$ graphene layers. As shown in Fig. 3 the voltage dependence of the differential resistance exhibits a series of eight peaks resembling the zero bias one and nearly equally spaced by $20 \pm 2$ mV. Their amplitude decreases with increasing voltage except for the broader peak at 50 mV which can be decomposed into two overlapping peaks centered around 40 and 60 mV. The periodicity of these oscillations is confirmed by Fourier transform; see Fig. 3. These oscillations are found to be nearly independent of temperatures up to 1 K.

The energy scale of 20 meV does not correspond to any simple electronic energy scale in the sample: the charging energy for a graphite sheet of length $L=3$ $\mu$m is roughly $e^2/\epsilon_0 L=5$ meV and the level spacing is $\hbar v_F/n_g L=30$ $\mu$eV. The characteristic Thouless energy for quantum interferences is smaller than $\hbar v_F/L=1$ meV which excludes any mesoscopic effect such as the ones reported in Ref. 13. Moreover any resonant tunneling or Coulomb blockade effect in an hypothetical double barrier structure of much smaller size than the sample can also be excluded since it would give rise to a Coulomb staircase with differential conductance *peaks* instead of the observed resistance *peaks* equivalent to conductance dips.[14] On the other hand the lowest energy optical phonon in graphite Z0' has an energy of 15 meV.[8] This mode, which emerges from the out-of-plane transverse acoustic mode of graphene,[8,15] is only present in multilayered samples and corresponds to two neighboring nonequivalent planes vibrating in phase opposition along the $c$ axis. This phonon mode has been detected experimentally in graphite by inelastic x-ray scattering[15] and scanning tunneling spectroscopy[16] with an energy of $\hbar\omega_0=15 \pm 1$ meV. The effect of this mode on the conductance should be particularly strong if the electronic transfer between the electrodes and the measured graphite foil takes place through different graphene layers on both sides of the sample.

Whereas in tunnel spectroscopy measurements [$\alpha=1$ in Eq. (1)] the anomaly in $dI/dV$ occurs at $\hbar\omega_0/e$, our experi-

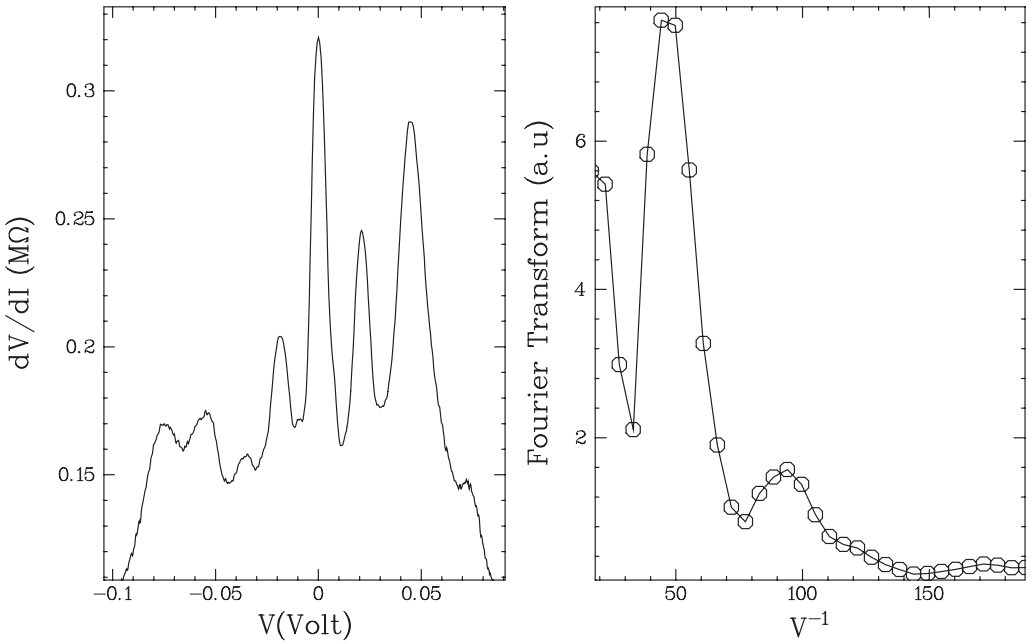


FIG. 3. Left panel: differential resistance of the 10-nm-thick suspended multilayer graphene sheet as a function of voltage bias measured at 60 mK. Right panel: Fourier transform of the signal showing the 20 mV periodicity.

mental configuration with two tunnel barriers is instead expected to give rise to a double structure both at $\alpha eV=\hbar\omega_0$ and $1-\alpha eV=\hbar\omega_0$ of respective weight $\alpha$ and $1-\alpha$. The observed peak positions at multiple values of 20 mV instead of 15 mV can thus be attributed to the asymmetry of the contacts with $\alpha \simeq 0.75$ in Eq. (1).[17] Note that STM spectroscopy on bulk graphite[16] also revealed inelastic contributions due to plasmons, which are not detected in the present experiment, as well as high energy optical phonon modes.

## III. DIFFERENTIAL CONDUCTANCE DATA ON FEW LAYER SUSPENDED SAMPLES WITH GATE

We have also investigated thinner suspended layers with only two or three graphene layers using a different fabrication process. They were fabricated by exfoliation of graphite flakes and deposition on a doped silicon substrate with a 285-nm-thick oxide. The number of layers was identified using Raman spectroscopy. The underlying silicon oxide was etched away in a hydrofluoric acid bath after contacting the samples with a bilayer of titanium gold by standard lithography techniques. These samples contain unfortunately much more defects than the thicker ones described above. We show in Fig. 4 the differential conductance on the data obtained on one of these samples with only two or three graphene layers. The data display closely spaced conductance dips and peaks at low energy and dips further apart at higher bias. We attribute the low bias features to energy level spacing in the sheet. The dips spaced 6–8 meV apart are attributed to the ZO' modes.

Contrary to the 10-nm-thick graphite sample discussed above there is indeed no clear separation in this very thin layer between the energy scales corresponding to the ZO' modes and the energy level spacing (of the order of 2 meV). This explains the existence of the low-energy peaks which positions depend on the gate voltage. Beside these low-energy features, dips at approximate multiple values of 8 meV are observed in the differential conductance. The Fourier transform of the signal exhibits a peak corresponding to this periodicity beside the main peak at 50 $V^{-1}$ previously observed. This finding is in agreement with the splitting of the ZO' mode predicted for the three graphene layers (see Ref. 18).

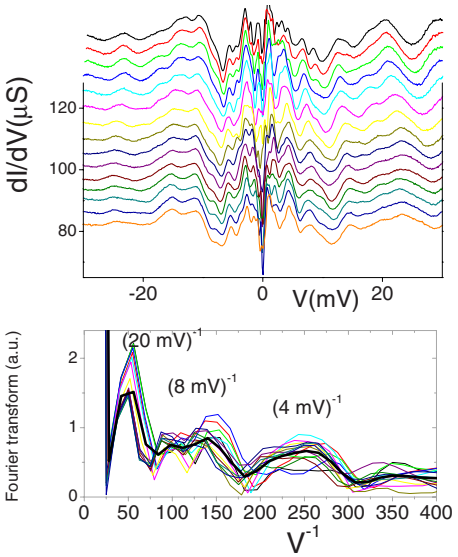


FIG. 4. (Color online) Differential conductance of a suspended trilayer graphene sheet as a function of bias measured at 60 mK for different gate voltages. The bold curve is obtained after averaging on the gate voltage. Fourier transform of the data revealing the 20 and 8 mV periodicities.

We emphasize that the conductance dips described above are only observed in thin suspended samples. They were not detected on the two thicker (more than 100 nm) samples. This can be understood considering that the conversion from electric energy (depending only on the resistance of the tunneling barriers) into mechanical vibrations induces vibrations whose amplitude is inversely proportional to the number of layers in the graphite foil. The suspended character of the sample is also essential since interaction with a substrate suppresses considerably the amplitude of induced vibrations, as demonstrated for carbon nanotubes.[3]

## IV. INTERPRETATION IN TERMS OF PHONON-ASSISTED DYNAMICAL COULOMB BLOCKADE

To explain the data more quantitatively we extended the work of Mitra *et al.*[7] on the phonon-assisted Coulomb staircase observed in transport through fullerenes molecules. The coupling between the ZO'-phonon mode and the electrons in the graphite sample is described using a Holstein Hamiltonian.[19] In the absence of disorder this Hamiltonian $H_G$ reads

$$H_G = \sum_k \epsilon_k c_k^+ c_k + \lambda \hbar \omega_0 \sum_k c_k^+ c_k (b^+ + b) + \hbar \omega_0 b^+ b, \quad (3)$$

where $c_k^+$ are $c_k$ are the fermionic electron creation and annihilation operators in momentum space, $\epsilon_k$ is the electronic energy, and $b^+$ and $b$ are the creation and annihilation operators of the bosonic ZO' phonon of frequency $\omega_0$. In contrast with previous work,[7] the electronic energy level spacing is small compared to the phonon energy $\hbar\omega_0$. The parameter $\lambda$ is the dimensionless electron phonon coupling constant which we take close to one like in carbon nanotubes.[20] The coupling to the leads is described in the dynamical Coulomb-blockade formalism,[9] by a tunnel Hamiltonian $H_T = \Sigma_{k,k'} T_{k,k'} a_k c_{k'}^+ e^{-i\phi} + \text{H.c.}$. Here $a_k$ are the electron annihilation operators in the leads, $T_{k,k'}$ are the tunnel amplitudes, and $\phi$ is a phase operator describing the electromagnetic environment of the junction. $H_G$ can be diagonalized with a canonical Lang-Firsov transformation: $b' = e^{-S} b e^S$, $H_G' = e^{-S} H_G e^S$ where $S = \lambda \Sigma_k c_k^+ c_k (b - b^+)$. In the limit of negligible charging energy[7] the transformed Hamiltonian reads simply $H_G = \Sigma_k \epsilon_k c_k^+ c_k + \hbar\omega_0 b^+ b$ where we omit the primes for the transformed operators. In the transformed basis $H_T$ is given by

$$H_T = \sum_{k,k'} T_{k,k'} a_k c_{k'}^+ e^{-i\phi + \lambda(b - b^+)} + \text{H.c.}. \quad (4)$$

This expression is obtained by expanding the product $e^{-S} H_T e^S$ under the assumption that the environment phase $\phi$ commutes with the phonon operators. It shows that the coupling to phonons essentially changes the phase operator of the junction. The current through the junction can thus be expressed with an effective $P(E)$ function describing the probability of electrons to lose an energy $E$ in a tunnel transition as in usual DCB theory.[9] Since the electromagnetic environment (em) and phonon operators commute, this function can be expressed as a convolution $P(E) = \int dE' P_{\text{env}}(E') P_{\text{ph}}(E - E')$, where $P_{\text{env}}(E)$ is the probability of emitting a photon of energy $E$ in the $RC$ environment of the junction and $P_{\text{ph}}$ is the probability of emitting a phonon in the sample. The probability distribution $P_{\text{ph}}$ can be obtained by analogy between the phase operator $i\lambda(b - b^+)$ with that of an (em) $LC$ circuit with resonant frequency $\frac{1}{\sqrt{LC}} = \omega_0$ (Refs. 9 and 10) [this can also be obtained by tracing out the phonon degrees of freedom in Eq. (4)]:

$$P_{\text{ph}}(E) = e^{-\lambda^2 \coth(\beta\hbar\omega_0/2)} \times \sum_k \delta(E - k\hbar\omega_0) e^{k\beta\hbar\omega_0/2} I_k\left(\frac{\lambda^2}{\sinh(\beta\hbar\omega_0/2)}\right), \quad (5)$$

where $\beta$ is the inverse of the phonon temperature $T_{\text{ph}}$ and $I_k$ is the Bessel function of order $k$. Using Eq. (A21) and standard expressions for current as a function of $P(E)$ (Ref. 9) one finds the differential conductance for one tunnel junction of resistance $R_T$:

$$\frac{dI}{dV} = \frac{1}{R_T}\left[\int_{-\infty}^{eV} d\epsilon P(\epsilon) + \int_{-\infty}^{-eV} d\epsilon P(\epsilon)\right]. \quad (6)$$

The case of an energy-dependent density of states and of asymmetric contacts can readily be included by generalizing this expression according to Eq. (1). For comparison with the experiments we take a density of states of graphite of the form $\nu(E) = \nu_0(1 + \frac{|E|}{\Delta})$. This formula is exact for bilayer graphene with $\Delta \approx 400$ meV (Ref. 21) and $|E| < \Delta$. We also take the values of $R_T$, sample resistance $R$, and charging energy deduced from the geometry and conductance data at low bias. The only adjustable parameter is the electron phonon (e-ph) coupling parameter which is found to be $\lambda = 0.7$. High (e-ph) coupling was already reported in graphene for in-plane optical modes.[22] In the present case, this large (e-ph) coupling between transverse ZO' vibrations and strongly anisotropic transport in the thin graphite layer can be understood if the electrical contacts between the two electrodes and the graphite foil take place through distinct graphene layers which is highly probable as mentioned above. As shown on Fig. 5 the agreement with experimental data is only qualitative especially at zero phonon temperature. Agreement is improved when a finite phonon temperature is included. This may describe the out-of-equilibrium phonon populations created by incoming electrons with a transfer rate $I/e = 10^{12}$ s$^{-1}$ larger than the phonon inverse lifetime $\omega_0/Q = 10^{11}$ s$^{-1}$. A quality factor $Q$ for the Z0' phonon of the order of 10 is indeed found in STM experiments.[16] These out-of-equilibrium effects as well as the value of $Q$ could moreover be enhanced in our suspended samples. We find that the best agreement between theory and experiment is obtained by imposing a bias-independent phonon temperature. This is probably due to the fact that we have not included the electron temperature and the broadening of the phonon mode due to the coupling to electrons.

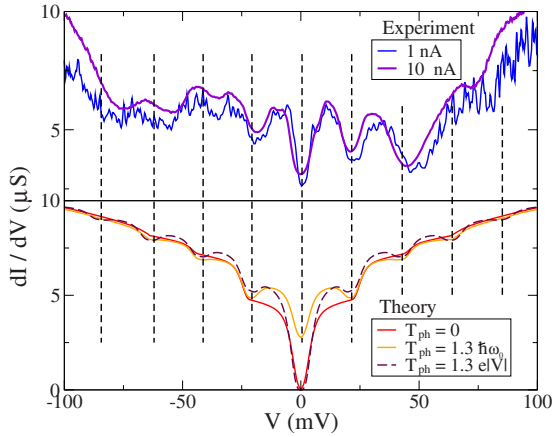


FIG. 5. (Color online) (upper panel) Differential conductance measured at 70 mK on the thin graphene foil depicted in Fig. 1, for to current excitations 1 nA (thin line) and 10 nA (bold line). Note the sharp dips nearly equally spaced by 20 mV, except the broad dip centered around 50 mV which can be decomposed into two overlapping dips centered around 40 and 60 mV as suggested by the data taken at 1 nA ac excitation. (lower panel) Theoretical fit for different phonon temperatures with the following parameters deduced from the geometry of the sample and the differential conductance data at low bias described by DCB: $\alpha=0.75$, $R_T=125$ kΩ, $\Delta=200$ mV, and $e^2/C=\hbar\omega_0/4$. The environment is described with a resistance $R/R_Q=1$. The only free adjustable parameter is $\lambda=0.7$.

## V. EFFECT OF MAGNETIC FIELD

In the following we discuss the magnetic-field dependence of the differential conductance dips (Fig. 6). They vary both in amplitude and position between 1 and 5 T. Whereas the first two dips and the fourth one are shifted toward lower voltage with increasing magnetic field (both at positive and negative bias) the third peak is shifted toward high frequency (we consider here the negative bias data since the second and third dips at positive bias can barely be resolved as discussed above). The conductance at the dips (inset of Fig. 6) either decreases or increases with magnetic field (dips 2 and 3), or varies in a nonmonotonic way (peaks 0 and 1). The typical amplitude of the relative shifts of the dips with magnetic field, typically 5%–20%, is of the same order of magnitude as the relative variation in the conductance on these dips. We attribute these effects to the field-dependent density of states of the graphite foil in the field range where Shubnikov de Haas (SdH) oscillations first appear. We understand qualitatively results of Fig. 6 taking into account the energy dependence of the frequency and amplitude of SdH oscillations. Above 1 T up to 5 T where the cyclotron frequency $\omega_c \simeq \omega_0$, this leads to field-dependent shifts both for the bias position $\delta V_n(B)$ and conductance value $\delta G_n(B)$ for the $n$th conductance dip at energy $\hbar\omega_n \simeq n\hbar\omega_0$. They differ both in sign and amplitude from peak to peak but have comparable relative magnitude (see the Appendix). Moreover, the Fourier transform of the differential conductance shows that the peak observed at 50 $V^{-1}$ for $B=0$ is clearly split at $B=5$ T. This splitting could be interpreted as the lifting of degeneracy between the cyclotron and the ZO' phonon resonances due to e-phonon interactions.[23]

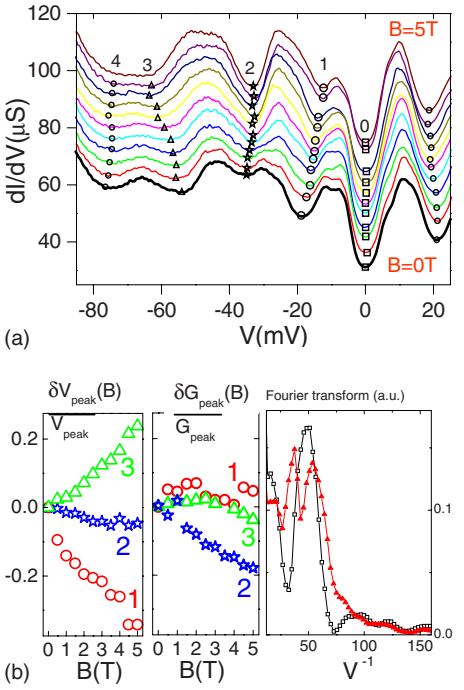


FIG. 6. (Color online) (a) Evolution of the differential conductance dips for different values of magnetic field. The different curves have been offset along the $Y$ axis for clarity. (b) On the left: field dependence of the bias positions of the dips labeled 1, 2, and 3. Center: value of conductance $\delta G=G(B)-G(0)$ measured at the minimum of these dips (same symbols). Right: Fourier transform of the differential conductance at $B=5T$ (triangles), compared to $B=0T$ (circles).

In conclusion we have found series of periodic dips in the differential conductance of suspended thin layers of graphite. These dips can be interpreted within a simple model of dynamical Coulomb blockade with an environment strongly coupled to the lowest energy optical phonon mode ZO' of graphite. The magnetic-field dependence of the effect observed when the cyclotron frequency is of the order of the frequency of the ZO' mode corroborates this interpretation.

## ACKNOWLEDGMENTS

We acknowledge M. Kociak for the transmission electron microscopy pictures, and J. N. Fuchs and M. Goerbig for fruitful discussions on the electron-phonon coupling in graphite. This work was supported by the EU-STREP program HYSWITCH.

## APPENDIX: $P(E)$ THEORY OF THE PHONON MODE

We consider the case of a single tunnel junction between a metallic lead (states with index $L$) and a graphite sample (states with index $S$) with coupling to an optical phonon mode with energy $\hbar\omega_0$ (operators of creation and annihilation $b^+$, $b$, and coupling constant $\lambda$). The interaction with the environment is described in terms of a phase operator $\phi$ as usually done in the dynamical Coulomb blockade theory. In the main text we have established that the electron-phonon

coupling can be absorbed in the tunnel Hamiltonian leading to

$$\hat{H} = \sum_L \epsilon_L a_L^+ a_L + \sum_S \epsilon_S c_S^+ c_S + \omega_0 b^+ b + \sum_{L,S} (t_{L,S} a_L c_S^+ e^{-i\phi - \lambda(b^+ - b)} + \text{H.c.}) \quad \text{(A1)}$$

$$= H_0 + H_T. \quad \text{(A2)}$$

From this Hamiltonian the transmission rates from state $|\epsilon_L, E_i, n_i\rangle$ to $|\epsilon_S, E_f, n_f\rangle$ can be determined using Fermi's golden rule. Here $\epsilon_L$ is the electron state in the lead and $\epsilon_S$ is the electron state inside the graphite sample; $E_i, E_f$ are the states of the environment and $n_i, n_f$ are the phonon modes;

$$\Gamma_{\epsilon_L, E_i, n_i | \epsilon_S, E_f, n_f} = \frac{2\pi|t|^2}{\hbar} |\langle E_i | e^{-i\phi} | E_f \rangle|^2 |\langle n_i | e^{-\lambda(b^+ - b)} | n_f \rangle|^2 \times \delta(\epsilon_L + E_i + \hbar\omega_0 n_i - \epsilon_S - E_f - \hbar\omega_0 n_f) \quad \text{(A3)}$$

where we have assumed that the transmission does not depend on energy.

The current is then expressed as

$$I = e \int d\epsilon_L \int d\epsilon_S \Gamma^{\Sigma}_{\epsilon_L | \epsilon_S} \nu_L(\epsilon_L) \nu_S(\epsilon_S) f(\epsilon_L - \mu_L) \times [1 - f(\epsilon_S - \mu_S)] - e \int d\epsilon_L \int d\epsilon_S \Gamma^{\Sigma}_{\epsilon_S | \epsilon_L} \quad \text{(A4)}$$

$$\nu_L(\epsilon_L) \nu_S(\epsilon_S) f(\epsilon_S - \mu_S)[1 - f(\epsilon_L - \mu_L)], \quad \text{(A5)}$$

$$\Gamma^{\Sigma}_{\epsilon_L | \epsilon_S} = \sum_{E_f, n_f, E_i, n_i} F_{\text{env}}(E_i) F_{\text{ph}}(n_i) \Gamma_{\epsilon_L, E_i, n_i | \epsilon_S, E_f, n_f}. \quad \text{(A6)}$$

Here $F_{\text{env}}(E_i)$ and $F_{\text{ph}}(n_i)$ are the occupation functions of the environment and of the phonon mode.

We now introduce the $P_{\text{env}}(E)$ function of the environment which is given by

$$P_{\text{env}}(E) = \sum_{E_i, E_f} F_{\text{env}}(E_i) |\langle E_i | e^{i\phi} | E_f \rangle|^2 \delta(E_f - E - E_i) \quad \text{(A7)}$$

and the $P_{\text{ph}}(E)$ function of the phonon mode, which we define by the expression

$$P_{\text{ph}}(E) = \sum_{n_i, n_f} F_{\text{ph}}(n_i) |\langle n_i | e^{-\lambda(b^+ - b)} | n_f \rangle|^2 \times \delta(\hbar\omega_0 n_f - E - \hbar\omega_0 n_i). \quad \text{(A8)}$$

With these notations we can compute the integral:

$$P(E) = \int dE' P_{\text{env}}(E') P_{\text{ph}}(E - E') = \sum_{E_f, n_f, E_i, n_i} F_{\text{ph}}(n_i) F_{\text{env}}(E_i) |\langle E_i | e^{i\phi} | E_f \rangle|^2 \quad \text{(A9)}$$

$$|\langle n_i | e^{-\lambda(b^+ - b)} | n_f \rangle|^2 \delta(\hbar\omega_0 n_f + E_f - E - E_i - \hbar\omega_0 n_i). \quad \text{(A10)}$$

Hence we find that

$$\Gamma^{\Sigma}_{\epsilon_L | \epsilon_S} = \frac{2\pi|t|^2}{\hbar} P(\epsilon_L - \epsilon_S). \quad \text{(A11)}$$

This leads to the following expression for the current:

$$I = \frac{2\pi|t|^2 e}{\hbar} \left\{ \int d\epsilon_L \int d\epsilon_S \nu_L(\epsilon_L) \nu_S(\epsilon_S) P(\epsilon_L - \epsilon_S) f(\epsilon_L - \mu_L) \times [1 - f(\epsilon_S - \mu_S)] - \int d\epsilon_L \int d\epsilon_S \nu_L(\epsilon_L) \nu_S(\epsilon_S) \times P(\epsilon_S - \epsilon_L) f(\epsilon_S - \mu_S)[1 - f(\epsilon_L - \mu_L)] \right\}. \quad \text{(A12)}$$

At zero temperature for constant density of states $\nu_S$ and $\nu_L$,

$$\int d\epsilon_L \int d\epsilon_S \nu_S \nu_L P(\epsilon_L - \epsilon_S) f(\epsilon_L - \mu_L)[1 - f(\epsilon_S - \mu_S)] = \nu_S \nu_L \int d\epsilon P(\epsilon)(eV - \epsilon)\eta(eV - \epsilon), \quad \text{(A13)}$$

where we have introduced $eV = \mu_L - \mu_S$.

After a similar development for the remaining term in Eq. (A12) we find that the current is given by

$$I = \frac{2\pi|t|^2 e \nu_S \nu_L}{\hbar} \int d\epsilon P(\epsilon)[(eV - \epsilon)\eta(eV - \epsilon) - (-eV - \epsilon)\eta(-eV - \epsilon)], \quad \text{(A14)}$$

where $\eta(.)$ is the Heaviside function.

The differential conductance reads for zero electronic temperature a single tunnel junction,

$$\frac{dI}{dV} = \frac{1}{R_T} \left[ \int_{-\infty}^{eV} d\epsilon P(\epsilon) + \int_{-\infty}^{-eV} d\epsilon P(\epsilon) \right], \quad \text{(A15)}$$

where

$$P(E) = \int dE' P_{\text{env}}(E') P_{\text{ph}}(E - E') \quad \text{(A16)}$$

and $P_{\text{ph}}$ is given by

$$P_{\text{ph}}(E) = \sum_{n_i, n_f} F_{\text{ph}}(n_i) |\langle n_i | e^{-\lambda(b^+ - b)} | n_f \rangle|^2 \times \delta(\hbar\omega_0 n_f - E - \hbar\omega_0 n_i). \quad \text{(A17)}$$

We notice that this sum corresponds to the $P_{LC}(E)$ distribution function for an *L-C* environment with resonant frequency $\omega_r = \frac{1}{\sqrt{LC}}$. Indeed it is shown in Ref. 9 that

$$P_{LC}(E) = \frac{1}{2\pi\hbar} \int dt \langle e^{i\psi(t)} e^{-i\psi(0)} \rangle_T e^{iEt/\hbar}, \quad \text{(A18)}$$

where $\psi(0) = \sqrt{g}(ia^+ - ia)$ with $g = \frac{e^2}{2C\hbar\omega_r}$, and $\psi(t) = e^{i\hbar\omega_r a^+ a} \psi(0) e^{-i\hbar\omega_r a^+ a}$. Here the operator $a^+$ and $a$ are photon creation/annihilation operators, and $\langle \ldots \rangle_T$ denotes thermal averaging over the thermal distribution $P_{LC}$ of the photon

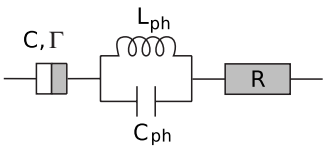


FIG. 7. Schematic representation of the graphite sample of resistance $R$ connected to a single tunnel junction characterized by its transmission $\Gamma$ and capacitance $C$. In the text we show that the phonon mode can be represented as an $LC$ circuit with parameters determined by $\frac{1}{L_{\rm ph}C_{\rm ph}}=\omega_0$ and $\frac{e^2}{2C_{\rm ph}\hbar\omega_0}=\lambda^2$.

modes in the resonator (Fig. 7). After inserting these expressions in Eq. (A18) we find

$$P_{LC}(E)=\frac{1}{2\pi\hbar}\int dt\sum_{n_i,n_f}P_{LC}(n_i)|\langle n_i|e^{-\sqrt{g}(a^+-a)}\times|n_f\rangle|^2e^{i(\hbar\omega_r n_i-\hbar\omega_r n_f+E)t/\hbar} \tag{A19}$$

$$=\sum_{n_i,n_f}P_{LC}(n_i)|\langle n_i|e^{-\sqrt{g}(a^+-a)}\times|n_f\rangle|^2\delta(\hbar\omega_r n_f-E-\hbar\omega_r n_i). \tag{A20}$$

After the substitution $\frac{1}{LC}=\omega_r=\omega_0$ and $g=\frac{e^2}{2C\hbar\omega_r}=\lambda^2$ Eq. (A20) has exactly the same form as Eq. (A17). We can now use the standard expression for $P_{LC}$ derived in Ref. 9 [Eq. (99)], which reads in terms of phonon parameters:

$$P_{\rm ph}(E)=e^{-\lambda^2\coth(\beta\hbar\omega_0/2)}\sum_k\delta(E-k\hbar\omega_0)\times e^{k\beta\hbar\omega/2}I_k\left(\frac{\lambda^2}{\sinh(\beta\hbar\omega_0/2)}\right), \tag{A21}$$

in this equation $\beta$ is the inverse phonon temperature.

In the case where the density of states in the sample $\nu_S=\nu_S(\epsilon_S)$ depends on energy, Eq. (A15) can be generalized to the following form:

$$\frac{dI}{dV}=\frac{\pi|t|^2\nu_L e^2}{\hbar}\left\{\int^{eV}d\epsilon P(\epsilon)\left[\nu_S\left(\frac{eV}{2}-\epsilon\right)+\nu_S\left(-\frac{eV}{2}\right)\right]+\int^{-eV}d\epsilon P(\epsilon)\left[\nu_S\left(\frac{eV}{2}+\epsilon\right)+\nu_S\left(-\frac{eV}{2}\right)\right]\right\}. \tag{A22}$$

This expression was derived from Eq. (A12) by assuming an asymmetric potential drop on the junction $\mu_L=eV/2$ and $\mu_S=-eV/2$. We notice that in general the conductance is an asymmetric function of the bias $V$, however, symmetry is recovered if the density of states $\nu_S$ is symmetric around the Fermi energy $\nu_S(V)=\nu_S(-V)$.

### 1. Density of states with emerging Landau levels

In presence of a magnetic field the density of states acquires an oscillating component as a function of energy

$$\nu_S(\epsilon)=\nu_S+\nu_1\cos\frac{\epsilon}{\hbar\omega_c},\quad \omega_c=\frac{eB}{m}. \tag{A23}$$

We will note $G_0(V)$ the value of $dI/dV$ for $\nu_1=0$ in absence of magnetic field. With this notation the general Eq. (A22) can be cast in the following form:

$$\frac{dI}{dV}=G_0(V)\left(1+\frac{\nu_1}{2\nu_s}\cos\frac{eV}{2\hbar\omega_c}\right)+\frac{\pi|t|^2\nu_L\nu_1e^2}{\hbar}\left[\int_{-\infty}^{eV}d\epsilon P(\epsilon)\cos\left(\frac{eV-2\epsilon}{2\hbar\omega_c}\right)+\int_{-\infty}^{-eV}d\epsilon P(\epsilon)\cos\left(\frac{eV+2\epsilon}{2\hbar\omega_c}\right)\right]. \tag{A24}$$

The origin of the peak's displacement can be understood on a heuristic level from just the first term of this equation,

$$\frac{dI}{dV}\sim G_0(V)\left(1+\frac{\nu_1}{2\nu_s}\cos\frac{eV}{2\hbar\omega_c}\right). \tag{A25}$$

We develop this expression around $V_n=n\hbar\omega_0$ where $G_0$ has a minimum (for simplicity we do not keep the second-order term in the development of the density of states);

$$\frac{dI}{dV}\simeq\left[G_0(V_n)+\frac{G_0''(V_n)}{2}(V-V_n)^2\right]\times\left\{1+\frac{\nu_1}{2\nu_s}\cos\frac{eV_n}{2\hbar\omega_c}-\frac{\nu_1 e}{4\nu_s\hbar\omega_c}\sin\frac{eV_n}{2\hbar\omega_c}\ (V-V_n)\right\}. \tag{A26}$$

This expression has a minimum at

$$V=V_n+\frac{\nu_1}{4\nu_S}\frac{e}{\hbar\omega_c}\frac{G_0(V_n)}{G_0''(V_n)}\sin\frac{eV_n}{2\hbar\omega_c}=V_n+\delta V_n, \tag{A27}$$

while the change in differential conductance at $V=V_n$ reads

$$\frac{dI}{dV}(V_n)=G_0(V_n)+G_0(V_n)\frac{\nu_1}{2\nu_s}\cos\frac{eV_n}{2\hbar\omega_c}=G_n+\delta G_n. \tag{A28}$$

In these equations we have introduced the notations $\delta V_n$ and $\delta G_n$ for the displacement of the peak and for the change in conductance. Combining the two previous equations leads to

$$\frac{\delta V_n}{V_n}=\frac{e}{2\hbar\omega_c V_n}\frac{G_0(V_n)}{G_0''(V_n)}\tan\frac{eV_n}{2\hbar\omega_c}\frac{\delta G_n}{G_n}(eV_n=n\hbar\omega_0). \tag{A29}$$

Thus the Shubnikov–de Haas oscillations in the density of states lead to a shift that depends on the peak position. In this calculation we have only taken into account the mixing between the differential conductance oscillations due to the presence of an optical phonon mode at energy $\hbar\omega_0$ and the oscillations due to the emergence of Landau levels in the density of states $\hbar\omega_c$. Such a mechanism is of course possible only in the regime where $\hbar\omega_0$ and $\hbar\omega_c$ have the same order of magnitude. Other effects may also contribute including broadening and energy displacement of the phonon mode in presence of magnetic fields.[24]

[1] A. Levy Yeyati and J. M. van Ruitenbeek, *Les Houches Session LXXXI, Nanophysics: Coherence and Transport*, edited by H. Bouchiat *et al.* (Elsevier, Amsterdam, 2005), pp. 495–535; O. Tal, M. Krieger, B. Leerink, and J. M. van Ruitenbeek, Phys. Rev. Lett. **100**, 196804 (2008).

[2] J. Park *et al.*, Nature (London) **417**, 722 (2002); H. Park *et al.*, *ibid.* **407**, 57 (2000).

[3] B. J. LeRoy, S. G. Lemay, J. Kong, and C. Dekker, Nature (London) **432**, 371 (2004).

[4] S. Sapmaz, P. Jarillo-Herrero, Y. M. Blanter, C. Dekker, and H. S. J. van der Zant, Phys. Rev. Lett. **96**, 026801 (2006).

[5] K. Flensberg, Phys. Rev. B **68**, 205323 (2003).

[6] S. Braig and K. Flensberg, Phys. Rev. B **68**, 205324 (2003).

[7] A. Mitra, I. Aleiner, and A. J. Millis, Phys. Rev. B **69**, 245302 (2004).

[8] L. Wirtz and A. Rubio, Solid State Commun. **131**, 141 (2004).

[9] G. L. Ingold and Y. V. Nazarov, in *Single Charge Tunneling*, NATO Advanced Studies Institute, Series B: Physics Vol. 294, edited by H. Grabert and M. H. Devoret (Plenum, New York, 1991); arXiv:cond-mat/0508728 (unpublished).

[10] T. Holst, D. Esteve, C. Urbina, and M. H. Devoret, Phys. Rev. Lett. **73**, 3455 (1994).

[11] P. R. Wallace, Phys. Rev. **71**, 622 (1947).

[12] A. Bachtold, M. de Jonge, K. Grove-Rasmussen, P. L. McEuen, M. Buitelaar, and C. Schonenberger, Phys. Rev. Lett. **87**, 166801 (2001).

[13] A. van Oudenaarden, M. H. Devoret, E. H. Visscher, Y. V. Nazarov, and J. E. Mooij, Phys. Rev. Lett. **78**, 3539 (1997).

[14] We do not think that the physics of cotunneling can describe our experimental results according to D. Averin *et al.*, Phys. Lett. A **140**, 251 (1989); and *Single Charge Tunneling*, NATO Advanced Studies Institute, Series B: Physics Vol. 294, edited by H. Grabert and M. H. Devoret (Plenum, New York, 1991); it would yield a $V^2$ dependence for the differential conductance instead of the power law with a small exponent that we observe.

[15] M. Mohr, J. Maultzsch, E. Dobardzic, S. Reich, I. Milosevic, M. Damnjanovic, A. Bosak, M. Krisch, and C. Thomsen, Phys. Rev. B **76**, 035439 (2007).

[16] L. Vitali, M. A. Schneider, K. Kern, L. Wirtz, and A. Rubio, Phys. Rev. B **69**, 121414 (2004).

[17] Note that beside the observed dips at multiples of $\hbar\omega_0/\alpha = 20$ mV a series of smaller dips by a factor 4 at multiples of $\hbar\omega_0/(1-\alpha) = 60$ mV are expected but cannot be resolved.

[18] Jia-An Yan, W. Y. Ruan, and M. Y. Chou, Phys. Rev. B **77**, 125401 (2008).

[19] T. Holstein, Ann. Phys. (N.Y.) **8**, 325 (1959).

[20] M. S. Dresselhaus, G. Dresselhaus, and P. C. Eklund, *Science of Fullerenes and Carbon Nanotubes* (Academic Press, San Diego, 1996).

[21] T. Ando, J. Phys. Soc. Jpn. **76**, 104711 (2007).

[22] A. H. Castro Neto and F. Guinea, Phys. Rev. B **75**, 045404 (2007).

[23] M. O. Goerbig, J. N. Fuchs, K. Kechedzhi, and V. I. Falko, Phys. Rev. Lett. **99**, 087402 (2007).

[24] J. R. Barker, J. Phys. C **5**, 1657 (1972).